



# Histological and proteome analyses of *Microbacterium foliorum*-mediated decrease in arsenic toxicity in *Melastoma malabathricum*

Sadiya Alka<sup>1</sup> · Shafinaz Shahir<sup>1</sup> · Norahim Ibrahim<sup>1</sup> · Norasfaliza Rahmad<sup>2</sup> · Norhazalina Haliba<sup>3</sup> · Fazilah Abd Manan<sup>1</sup>

Received: 14 November 2020 / Accepted: 31 May 2021 / Published online: 16 June 2021  
© King Abdulaziz City for Science and Technology 2021

## Abstract

Arsenic (As) is an increasing threat across the globe, widely known as a non-threshold carcinogen, and it is reaching harmful values in several areas of the world. In this study, the effect of plant growth promoting bacteria (*Microbacterium foliorum*) on inorganic arsenic (Arsenate) phytoremediation by *Melastoma malabathricum* plants was investigated through histological analysis and proteome profiling of the *M. malabathricum* plants. Two-dimensional gel electrophoresis and transmission electron microscopy were used to conduct the proteome and histological analysis. When arsenic-treated cells were compared to untreated cells, substantial changes were found (1) severely altered the morphology of the cells, intensely disturbed; (2) the cell wall was thicker; (3) drastically changed the cytoplasm, the cells were polygonal in shape, different in size (scattered), and relatively dense. Compared to the control group, the ultra-structure of the root cells of the control group revealed intact cytoplasm, vacuole, and cell wall under exposure to As + bacteria that had a minor effect on the cell form. To further understand As + bacteria interaction, proteome profiling of the root cell was analyzed. The As-induced oxidative stress enrichment was confirmed by the up-regulation of tubulin, nucleoside diphosphate kinase, and major allergen during As + bacteria exposure. It was observed that the profusion of proteins involved in defence, protein biogenesis, signaling, photosynthesis, nucleoside and energy metabolism was greater in As + bacteria as compared to the rooting out of As only. Overall, it can be obviously seen that the current study demonstrates the effectiveness of phytoremediation by *M. foliorum* on proteins involved and responsive pathways in dealing with As toxicity in *M. malabathricum* plant.

**Keywords** Histological observation · Protein profiling · *Microbacterium foliorum* · *Melastoma malabathricum*

## Introduction

Arsenic (As) contamination of the environment is fast becoming a global problem originating from anthropogenic activities such as urbanization, metal mining, rapid industrialization, and inorganic fertilizers and other agrochemicals

(Alka et al. 2020, 2021; Chauhan et al. 2020). Mining activities and various heavy industries are important economic sources for Malaysia, with most of the urban regions and industries found in the western part of the country (Ahmadpour et al. 2012; Rajoo et al. 2013). The common origin of As contamination in Malaysian soils is pesticides, manufacturing industries, abandoned mining sites, and inappropriate waste recycling.

Arsenic is mostly found in the soil in two inorganic forms as oxyanions of trivalent Arsenate (AsIII) or pentavalent Arsenate (AsV). Arsenite (III) is more mobile and toxic to living organisms than Arsenate (V) (Squibb and Fowler 1983; Srivastava et al. 2011). However, the best available form of arsenate is found in oxygenated ecosystems: aerobic soils and superficial water. Since arsenate is a phosphate chemical analog, it can be simply assimilated by plants via phosphate transporters with a high affinity in their roots (Fru

✉ Fazilah Abd Manan  
m-fazilah@utm.my

<sup>1</sup> Department of Biosciences, Faculty of Science, Universiti Teknologi Malaysia, 81310 Skudai, Johor, Malaysia

<sup>2</sup> Agro-Biotechnology Institute, National Institutes of Biotechnology Malaysia (NIBM), c/o MARDI Headquarter, 43400 Serdang, Selangor, Malaysia

<sup>3</sup> University Industry Research Laboratory, Universiti Teknologi Malaysia, 81310 Skudai, Johor, Malaysia

et al. 2018; Fu et al. 2009). Thus, human health is at risk by consuming crop plants that have accumulated arsenate (Lindsay and Maathuis 2017). This is increasingly evident in substantial progress made in recent years concerning molecular evidence on arsenic absorption and, in particular, the role of specific proteins in the availability of arsenic to seeds and grains (Lindsay and Maathuis 2017). The pollutant activates severe alterations in the plant's metabolism once it is absorbed. Both biochemical and physiological processes become affected, thereby leading to alterations in cell morphology and organization of the plant (Farnese et al. 2017).

Most As-triggered damages in plants are due to reactive oxygen species (ROS) higher production, which can interact with most molecules, thereby modifying their functions and structure, leading to the obstruction of the plant survival and growth (Ahmad et al. 2020; Farooq et al. 2018a, b). Excess ROS has also been found to disrupt normal plant metabolism by damaging oxidative processes tremendously, nucleic acids, proteins, lipids, irreparable damage to DNA and various cell organelles, including chloroplast (Long et al. 2019; Ghosh et al. 2021). In the root cells, As(V) and phosphate create interference in the metabolic pathway as they compete for the same transporter. Several plants were verified to mount up toxic metalloids in their above-ground biomass, which lead to a decrease in crop yield and productivity, ultrastructural alteration, oxidative stress, and decrease in protein content in As-contaminated areas (Das et al. 2014; Ghosh et al. 2021). Numerous conventional remediation approaches have been used to reduce the uptake of heavy metals in plants that are burdened with toxic secondary products and huge monetary investments (Zaheer et al. 2020). The development of cost-effective bioremediation techniques provides a much-needed stimulus to increase crop production in contaminated metalloid soil. Plant growth-promoting bacteria and root-colonizing soil bacteria that exert growth-promoting properties are well adapted to adverse environmental conditions. This property helps them increase plants' growth and development and, thus, reduce the detrimental effects of various environmental stress that can hinder plants' survival and productivity (Ghosh et al. 2021). Numerous As-resistant bacteria have been identified by multiple researchers (Bahari et al. 2017; Del Giudice et al. 2013; Pandey et al. 2020; Vezza et al. 2020) to have the ability to reduce As(V) to As(III).

The combination of plants and microbes can improve the efficiency of phytoremediation. *M. foliorum* sp. strain SZ1 is a genus of *Microbacterium* from the family *Microbacteriaceae*. The *Microbacterium* has 96 species. They are gram positive (Corretto et al. 2015), which are essential in agriculture (Behrendt et al. 2001) and contribute a lot to the soil system. For example, they help the plant by fixing nitrogen in the soil in exchange for plant saccharide (Behrendt et al. 2001). *M. foliorum* sp. strain SZ1 is the first As resistance

bacteria isolated in Malaysia from the ex-gold mining site, highly contaminated with As (Bahari et al. 2017). These bacteria can tolerate As toxicity at a half-maximal inhibitory concentration (IC50) of 140 mM (Bahari et al. 2017).

Microbe-assisted bacteria and *M. malabathricum* for As removal and its effect on the physiological, biological, and metabolic response of the plant are still at an early stage. Therefore, this study focuses on the histological and proteome changes of *Microbacterium foliorum*-mediated decrease of arsenic toxicity in *M. malabathricum*.

## Materials and methods

### Plant growth and experimental background

The study was conducted in a greenhouse environment under controlled conditions (such rain and too much sunlight) at the Faculty of Science of the Universiti Teknologi, Malaysia, Johor campus. *M. malabathricum* was bought from a nursery at 1 month old and were grown for 3 months in sterile soil until they reach a certain height (15 cm in height) and transferred to experimental pots with one plant per pot (2.5 L) containing a mixture of sterile soil (2 mm sieved) and sandy soil for better drainage and leaching under greenhouse conditions. Depending on the greenhouse condition, all pots received natural light, day–night humidity 70/90%, and not temperature controlled, and irrigation activity was carried out regularly as needed. Four replications make 88 pots in a fully randomized design and treatment group details (Tables 1 and 2). In all treatment groups, As concentration was determined before the start of the pot experiment.

The sterilized soil was spiked with an arsenic source, soluble arsenic salt ( $\text{Na}_2\text{HASO}_4 \cdot 7\text{H}_2\text{O}$ ), in 100 mL of distilled water (Dadrassnia and Pariatamby 2016). As solutions (0, 50, 70 ppm) were thoroughly mixed with the whole amount of the soil (Tlustoš et al. 2002) and As leachate was collected (Titah et al. 2013) throughout the analysis. For analysis, soil samples were collected from each pot before and after treatment.

**Table 1** Treatment groups with *M. malabathricum*

Treatment groups	Identified as
A1	As-contaminated soil with the addition of microbes
A2	As-contaminated soil without addition of microbes
A3	Control

**Table 2** Treatment groups without *M. malabathricum*

Treatment groups	Identified as
A4	As-contaminated soil with the addition of microbes
A5	As-contaminated soil without addition of microbes
A6	Control

Three-month-old plants (well-rooted matured from the same batch and age) were transplanted and allowed 2 weeks to adapt before the microbial inoculation. The microbial solution was formulated in 10 mL distilled water suspended from  $10^8$  CFU/mL per microbe and applied uniformly on the soil around the roots of plants according to the techniques demonstrated by Mukherjee et al. (2018). The plants were grown for 90 days in the greenhouse and subsequently harvested to estimate various plant parameters.

### Plant growth promoting bacteria (PGPB) culture preparation

*Microbacterium foliorum* sp. strain SZ1 previously isolated from As-contaminated soil was cultured overnight and colonies harvested. The microorganisms were washed twice in sterile distilled water and re-suspended in autoclaved distilled water until the final OD (600 nm) of 1.0 was achieved (about  $10^8$  CFU/mL). The bacterial suspension of 1 mL was inoculated onto the treated pot near the root of the plant.

### Root tissues histological study with transmission electron microscopy (TEM)

Root sections (~ 2.0 mm) were quickly submerged in H<sub>2</sub>S saturated water as pre-treatment for approximately 30 min in a comfortable temperature range indoors (Khan et al. 1984). The samples were cleaned using 0.1 M SCB (the buffer of sodium cacodylate, alkalinity of 7.4) and further submerged in 2.5% glutaraldehyde (v/v) readied in sodium cacodylate, buffer (pH 7.4) for a period of 2 h at 4 °C. Samples of the tissue were cleaned 3 times using 0.1 M SCB and a 10-min lapse was taken from every cleaning to determinate at 1% OsO<sub>4</sub> (osmium tetroxide) over a 24-h period. Having done that, SCB was utilized to wash the fixed tissue. Subsequently, the fix tissue was then dried up in graded acetone series (35, 50, 70, 95, and 100%) embedded in the mixture of Araldite–DDSA. Having baked at 60 °C, ultramicrotome (RMC Boeckeler PowerTome PC, Boeckeler Instruments, USA) was utilized to cut blocks (60–80 nm thick) after

marking the sections with lead citrate and uranyl acetate. The sections were examined using a 120 kV high-resolution transmission electron microscope (Hitachi HT-7700, Japan).

### Protein extraction, quantification and identification by liquid chromatography–tandem mass spectrometry

Using the Bradford assay, the amount of protein extracted from *M. malabathricum* was determined. First, using the Amersham kit (Bovine Serum Albumin, BSA) at blank against its absorbance, a standard curve with known protein concentration was plotted. By diluting the extracted protein with 500 µL of Bradford reagent, the standard solution was prepared with the extracted protein and allowed to remain for 20 min. After 20 min, the absorbance at 595 nm was read, recorded and the protein concentration measured in accordance with the plotted standard curve.

### Rehydration

DTT 7 mg/mL was applied, vortexed, centrifuged and pipetted onto a strip holder after the sample was cleaned-up and sonicated for 1 h at 37 Hz. The tape was removed on the 7 cm ReadyStrip IPG (pH 3–10, non-linear; Bio-Rad, CA, USA) or 18 cm pH gradient (IPG) strips (pH 3–10 non-linear; Amersham, GE Healthcare Bio-sciences, Sweden) and placed gel side down on the protein sample to ensure that no bubbles between the protein sample and the IPG strip were created. The cover fluid was then applied and submerged in the strip. The strip holder was covered with aluminum foil and left to be rehydrated overnight.

### Isoelectric focusing

The protein was separated by an isoelectric point (pI) in an electric field in this step. Two wicks were moistened with distilled water on either side and placed inside the electrode tray. Then, according to the electrode end, the rehydrated IPG strip was then placed in gel side down in the electrode tray, and cover fluid was then used to cover the strip. Subsequently, the electrode tray was covered and put into the PROTEAN IEF Cell (Bio-Rad, USA) and the IEF method was specified.

### Equilibration and gel run

The electrode tray was removed from the PROTEAN IEF Cell (Bio-Rad) after completion of the IEF, and the strips were transferred upside down to a strip holder gel. SDS equilibration buffer (6 M urea, 75 mM pH 8.8 Tris HCl, 29.3% (v/v) glycerol, 2% (w/v) SDS, 0.02% (w/v) bromophenol blue) with DTT (100 mg/10 mL) was first added, then SDS

equilibration buffer with iodoacetamide (250 mg/10 mL) was used and the strip holder was shaken for 15 min on a gyro-rocker. Then the IPG strips were cut and put in the 2D GE, and the well was perfused with 5  $\mu$ L of protein marker. To seal the strip and protein marker, an agarose sealing solution (25 mM Tris base, 192 mM glycine, 0.1% (w/v) SDS, 0.5% (w/v) agarose, 0.002% (w/v) bromophenol blue) was used. The gel was then put in the chamber of electrophoresis and ran at 100 V until the front dye reached the bottom of the gel.

### Image acquisition and data analysis

Using the Bio-Rad FluorS device that has a 12-bit sensor, the silver tained gel collected following 2DE was screened for imaging. For data analysis in PDQuest version 8.0.1 (Bio-Rad), images obtained from four replicated 2-DE gels were used. Using the techniques demonstrated by Agrawal et al. (2013), parameters such as protein spot consistency, molecular mass, and discrete protein pI were examined. For this study, points showing quality and quantity reproducibility in at least two of the three replication gels were considered. To prevent experimental differences in gels due to protein load or staining, a normalized spot volume for protein quantification was obtained by PDQuest software following the total spot volume standardization protocol.

### Liquid chromatography–tandem mass spectrometry

Using the EASY-nano liquid chromatography (EASY-nLC) 1200 System (Thermo Scientific, MA, USA), the Q Exactive Plus Hybrid Quadrupole-Orbitrap mass spectrometer (Thermo Scientific, MA, USA) was linked to separations and spectrum acquisitions of protein digests. For 20  $\mu$ L, 0.1% FA and 5% ACN, tryptic digests were redissolved in an Acclaim PepMap 100 C18 reversed phase column (3  $\mu$ m, 0.075  $\times$  150 mm) (Thermo Science, MA, USA) for peptide separation, a sample volume of 2  $\mu$ L was applied. With 95% mobile phase A (0.1% FA) and 5% mobile phase B (0.1% FA in ACN), the column was held at equilibrium. To elute the bound peptides at a flow rate of 300 nL min<sup>-1</sup>, a gradient of 5–35% mobile phase B in 70 min was used. Gas-phase peptide ions were generated with a spray voltage of 1800 V by electrospray ionization. The Orbitrap mass analyzer performed a peptide precursor survey scan with a mass range of  $m/z$  310–1800 and a resolving power of 70,000. This was accompanied by the application of a cumulative injection time of 100 ms. For tandem MS (MS<sup>2</sup>), peptide precursors were selected with charge states of 2–8. With the linear ion trap mass analyzer, which has a resolution power of 17,500, 0.7  $m/z$  isolation window and a maximum injection time of 60 ms, Tandem MS conditions were rapid scan rate. Precursors were separated into fragments using collision induced

and high-energy collision induced (CID and HCD) at a normalized collision energy of 28%, respectively. The scanned mass range ranged from  $m/z$  110 to 1800. Via the PRIDE (Perez-Riverol et al. 2019) partner repository with the dataset identifiers PXD013255 and 10.6019/PXD013255, the mass spectrometry proteomics data were deposited to the ProteomeXchange Consortium.

### Data analysis

Thermo Scientific Xcalibur (Version 4.1.31.9) (Thermo Scientific, MA, USA), data collections were conducted in positive mode. Thermo Scientific Proteome Discover, version 2.1 (Thermo Scientific, MA, USA) was analyzed with raw data (RAW) to generate peak lists in DTA format for database searching. Tandem (MS<sup>2</sup>) mass spectra were searched in the NCBI protein database with the SEQUEST HT engine against *Elaeis guineensis* (TaxID = 51953) and *Phoenix dactylifera* (TaxID = 42345) taxonomies (containing 35,972 and 33,101 protein sequences as of 30 October 2017, respectively). Mass tolerances were set to 20 ppm and 0.5 Da for the peptide and product ions. With two missing cleavages allowed, Trypsin was selected as the protease. Carbamidomethylation was developed as the fixed modification for cysteine and lysine, while methionine oxidation and asparagine and glutamine deamidation were used as variable modifications. Proteins with a peptide of at least one rank were approved. A decoy database included randomized sequences of taxonomies searched for. To calculate the false discovery rate, all database searches were also carried out against the decoy database. A Percolator version 2.04 (Proteome Discover component) based on q-value at a 1% false discovery rate was authenticated for all peptide spectral matches. With the support of a free web-based software (<http://bioinformatics.psb.ugent.be/webtools/Venn/>), the Venn diagram of the defined proteins from the evaluated solubilization buffers was created. In Uniprot (<https://www.uniprot.org/uploader/dlists/>), the biological process, cellular portion and molecular structure of the identified proteins were annotated using the Retrieve/ID mapping method. The Uniprot-GOA database (<http://www.ebi.ac.uk/GOA>) collected Gene ontology (GO) terms associated with the known proteins from all the measured solubilization buffers.

### Supervised partial least squares discriminant analysis (PLS-DA)

To analyze the correlation of the established proteins and different solubilization buffers, supervised PLS-DA using MetaboAnalyst 4.0 (<http://www.metaboanalyst.ca/>) (Xia et al. 2015) was adopted. Data inputs containing the calculated  $m/z$  value for each peptide were extracted from the Thermo RAW files and their corresponding retention time

and strength. A total of 93,777 peaks, with an average of 5861.1 peaks per sample, were used for four replicates representing each of the measured solubilization buffers. This was accompanied by a summation of peaks from the same sample belonging to the same group, resulting in 5483 peak groups. These variables were constructed according to their retention time, matching the peaks. Mass and retention time were changed, respectively, to 0.025  $m/z$  and 30 s. The unusable variables (Hackstadt and Hess 2009) were filtered out by interquartile range (IQR) to strengthen the regression model. The uninformative regions or noise of mass spectra are usually these variables. Using the number of intensities and Pareto scaling (Van den Berg et al. 2006), the model interpretation was improved by normalizing the datasets, normalization and data scaling based on data dispersion were carried out. Due to the dynamism of the produced proteomics data, Pareto scaling (square root of the standard deviation as the scaling factor) was applied (Wheelock and Wheelock 2013; Worley and Powers 2013). As PLS-DA tends to overfit results, the statistical model was authenticated using a permutation test (Barberini et al. 2016; Bijlsma et al. 2006). The importance of the differences between the buffers evaluated was determined by this test. There were 1000 permutations of the Y-block (class assignment). For the class assignment forecasts, a sum of squares between/within ( $B/W$ ) ratio was calculated for every PLS-DA model developed. In a histogram, these ratios were plotted. Looking at this statistically, the more the  $B/W$  ratio of the original class assignment to the

authorized class assignment distribution is to the right, the greater the difference between the two class assignments.

## Statistical analysis

One-way ANOVA was employed to examine the variations between the treatments. In proteomic analysis, the intensity of the spot of the differential protein in 2-DE gel was found out from the replicate gel, 4 spots as well as a minimum 1.5-fold increase or decrease in protein expression were considered for differential spot recognition between different treatments.

## Results and discussion

### Histological observation of *M. malabathricum* roots after treatment

The ultra-structure of the root cells surveyed with a High-Resolution Transmission Electron Microscope 120 kV (Hitachi HT-7700, Japan) is shown in Figs. 1, 2, 3, 4 and 5. In the structural organization of cells from various treatment groups, findings showed similar and differential characteristics with low (2  $\mu\text{m}$ ) and high (5  $\mu\text{m}$ ) magnifications. There were some structural characteristics of cells with different As concentrations (untreated, As-stressed and As + bacteria) and had several variations that characterized their structural organization. Untreated cells (Fig. 1), As-stressed cells (Figs. 4, 5) and As + bacterial cells (Figs. 2, 3) have shown

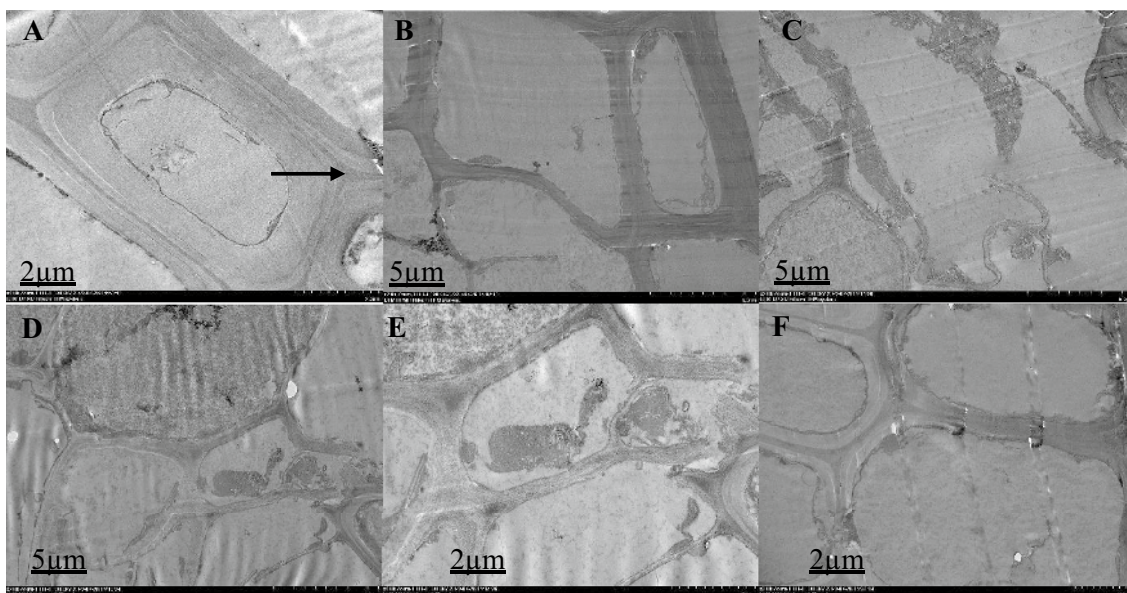


**Fig. 1** Ultrastructural organization of *M. malabathricum* roots, TEM images showing the cell wall, nuclear membrane, nucleus and vacuole. Tissue samples were obtained after 90 days of exposure in con-

trol soil (A3). Thick arrow shows the cell wall (A), higher magnification observed cell structure: relative to other treatment groups, the cell structure appears to be usual (B–F)

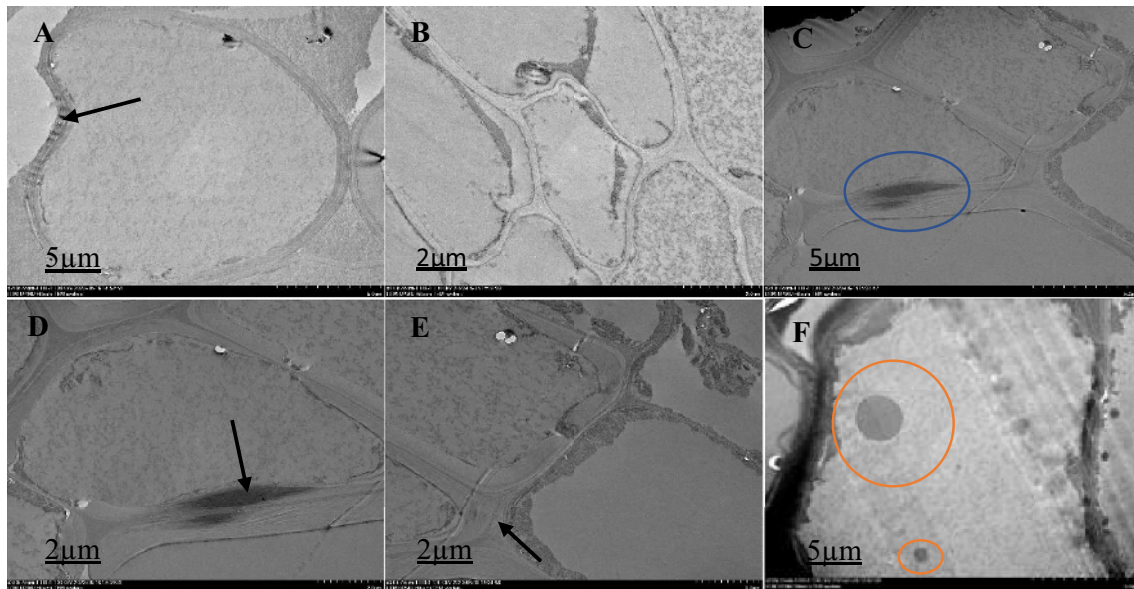


**Fig. 2** Ultrastructural organization of *M. malabathricum* roots, TEM images showing the cell wall, nuclear membrane, nucleus and vacuole. Tissue samples were obtained after 90 days of exposure to 50 ppm As + bacteria in soil. Thick arrow shows cell wall (A, D and E), blue circle showing unidentified image (C), red circle shows elec-

tron dense material (F), higher magnification observed cell structure: extracellular dark deposits are observed in several cells in contact with the outer face of the cell walls, some two-cell structures showing different asymmetric location of the dividing cell wall and some specifics of the organization of the cell (B)

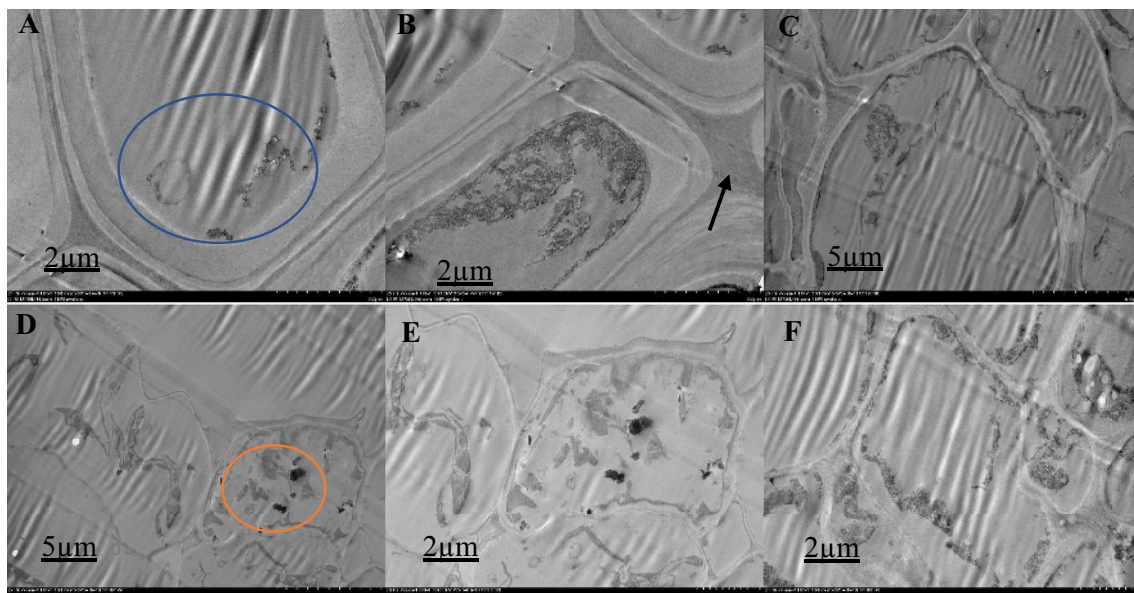


**Fig. 3** Ultrastructural organization of *M. malabathricum* roots, TEM images showing the cell wall, nuclear membrane, nucleus and vacuole. Tissue samples were obtained after 90 days of exposure to 70 ppm As + bacteria in soil. Thick arrow shows cell wall (B), blue circle shows unidentified structure (A, C), red circle shows electron

dense material (D, E). Higher magnification of the specifics of the cell organization; chloroplasts with a rounded form and smaller size with a denser internal membrane structure, cells with a polygonal shape, various sizes (scattered) and relatively dense (F)

that, compared to As-stressed cells under As and bacterial exposure, the ultra-structure of control root cells displayed intact cytoplasm, vacuole and cell wall that had a marginal

effect on cell structure. Chloroplasts, cell walls, vacuoles and extracellular deposits were affected by the key differences found between the cell types in the treatment group,

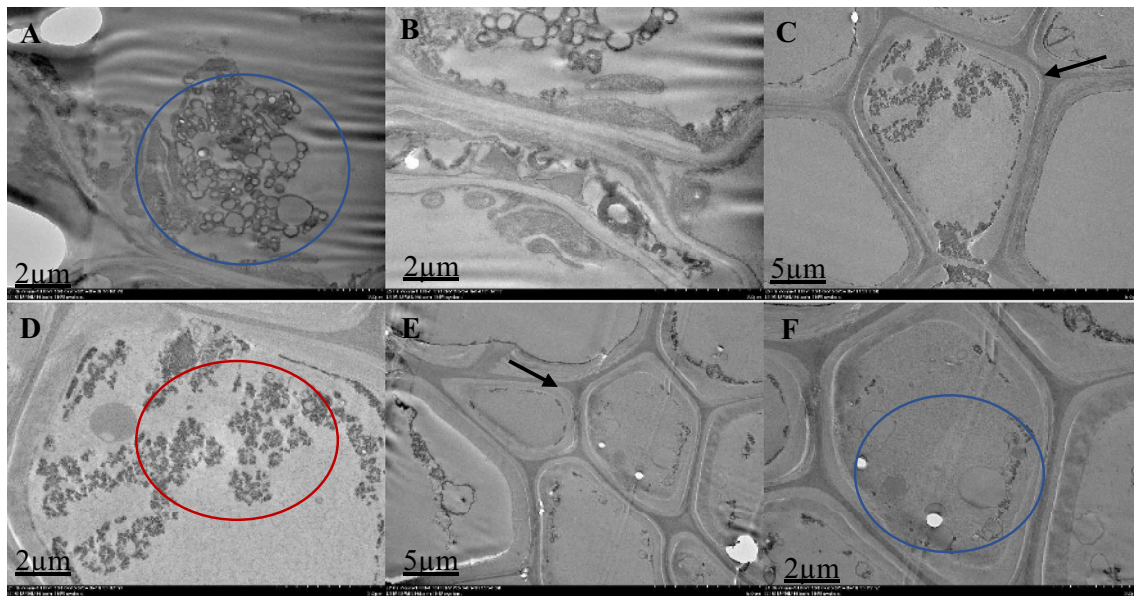


**Fig. 4** Ultrastructural organization of *M. malabathricum* roots, TEM images showing the cell wall, nuclear membrane, nucleus and vacuole. Tissue samples were obtained after 90 days of exposure to 50 ppm As in soil. Thick arrow shows cell wall (C and E), blue circle shows unidentified structure (A, B and F), red circle shows elec-

tron dense material (D). Higher magnification of the specifics of the cell organization; some two-cell structures showing the dividing cell wall's distinct asymmetrical location and certain cell organization features. Chloroplasts with denser-structured internal membranes showed a rounded shape and smaller scale

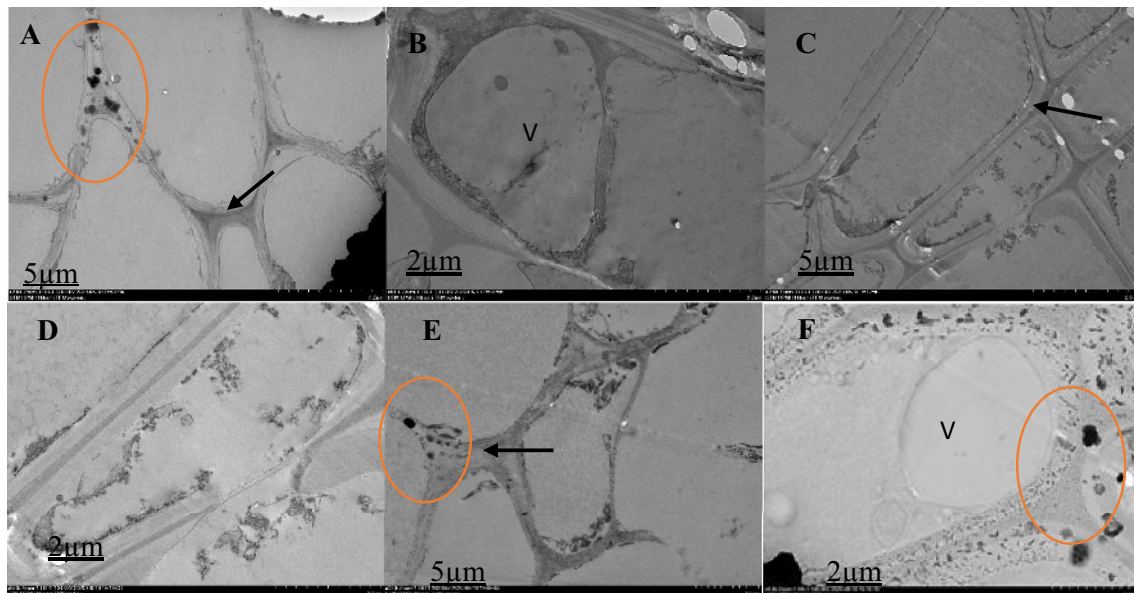


**Fig. 5** Ultrastructural malabathricum root organization, TEM photos illustrating the cell wall, nuclear membrane, nucleus, and vacuole. After 90 days of exposure to 70 ppm of arsenic in the soil, tissue samples were taken. Thick arrow shows cell wall (A, C and E), red circle shows thick electron content (A, D and F), V=vacuole (B). Higher

magnification of the specifics of the cell organization; extracellular dark deposits (red circle) are found in many cells in contact with the outer face of the cell walls; cells show large vacuoles (V). On the cell walls, extracellular deposits of various sizes and types (rounded and ellipsoid) are found

whereas the cell walls were thicker than in the control group. However, after 90-day treatment with the As stress, there were drastic changes in cytoplasm, cells were polygonal

in shape, different in sizes (scattered) and relatively dense. The organelles were undistinguishable, especially for As-stressed (50 ppm) groups, cell morphology was severely

altered, intensely disrupted. The degradation of the nuclear envelope and leakage of the nuclear contents were clearly exhibited. Numerous dark and small rounded deposits were found attached to the outer surface of the cell wall in As-stressed cells (Fig. 5). The other treatment group' cells did not exhibit identical extracellular characteristics. The longitudinal cells with large vacuoles contain electron dense material and rounded cells with thin cell wall (Fig. 5). As-stressed cells (Fig. 5B, F) showed abnormal shape, most of them with a large cytoplasmic vacuole occupying a high proportion (~ 15–25%) of the cellular volume compared to other treatment group.

The present study revealed that the root showed changes under stress (50 and 70 ppm) in separate cell organelles (Figs. 1, 2, 3, 4 and 5). This study also provided information about the As-induced effects that follow a long-term response associated with adaptive processes on the *M. malabathricum* cell structure. Cells accumulated high As concentrations when they were grown in soil with As + Bacteria no toxicity symptoms, in agreement with previous results (Farooq et al. 2018a, b). The investigation of the ultrastructural alterations in As-stressed plant cells would be a means and useful instrument in designing the accurate mechanisms utilized in As-tolerance conferment. ROS as a stress indicator acts on intracellular organelles, proteins, enzymes, nucleic acids; however, ROS generation's pathway and intensity are determined by the conditions of stress and organelles of cell (Khan et al. 2020). Several changes were observed in the ultra-structure cells root under As stress (Alcantara-Martinez et al. 2016; Farooq et al. 2018a, b). The root cell under As stress depicted the changes in different cell organelles including vacuole. Several characteristics that may obviously be seen clearly in the two plants were nucleolus loss, nuclear membrane as well as nucleus disruption, and in addition to vacuole size getting larger. High concentrations of As absorption and accumulation causes cytotoxic effect in some plant species, causing structural and ultrastructural changes that affected plant growth and physiological well being (Farooq et al. 2016). The roots take in water and vital elements from the earth and, thus, change in their biochemistry and ultramorphology. This may lead to the obstruction of the plant's growth. The cellular and subcellular level heavy metal distribution is significantly more important for heavy metal removal and accumulation in plants (Zhou et al. 2016). Studies have shown that the first barrier to the absorption of metal ions into cells is the effect of arsenic on the cell wall (Farooq et al. 2016), a similar mechanism to the accumulation of arsenic in barley, where arsenic was mainly accumulated in the root cell wall (Zvobgo et al. 2018). The results also showed that As exposure induced changes in subcellular structures, such as chloroplast compartment. It was reported to affect chloroplast and its internal membranes. It can, therefore, reduce

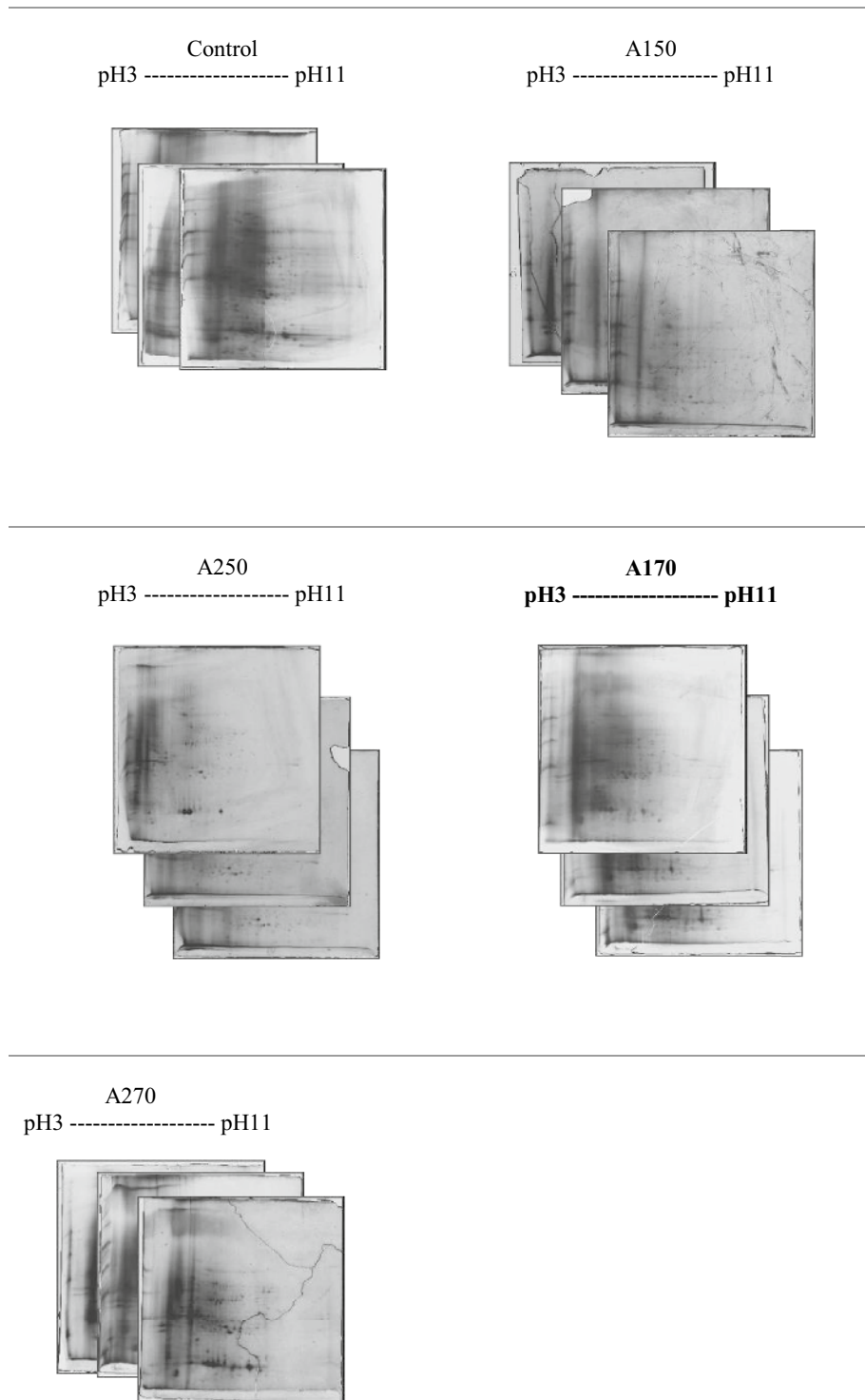
the photosynthetic pigments concentration and consequently lessening the assimilation rates of carbon.

In this study, we show that in As-stressed cells, the vacuole increases and the aggregation of electron dense granules occurs. The enlarged and increased number of vacuoles has been reported due to As effect on the roots (Farooq et al. 2018a, b; Khan et al. 2020). Number of electron dense granules and crystalline structures were attached to the cell walls and present in the vacuoles. One of the plants features against the exposure of As is the precipitation of electrons dense materials in cellular compartments (Alcántara-Martínez et al. 2018) and other toxic metals like lead, chromium and cadmium (Chandrasekhar and Ray 2019; Khan et al. 2020; Samrana et al. 2020), whereby it is replicated in among the earliest cellular mechanism upon the phytotoxicity of metal (Hall 2002). Samrana et al. (2020), reported that the extent of heavy metal in vacuole surpassed its reposition boundary and can upset the cytoplasm. This can result to a peculiar and condensed structure and, in addition to dented membranes, chiefly tonoplast. Additionally, it might be resulting from the disparity in the production of ROS in cell organelles. Earlier studies have reported that the damage of the root cells of *Brassica napus* and *Hordeum vulgare* is a result of the stress of heavy metal (Ali et al. 2013; Khan et al. 2020). This study shows that the As + bacteria have reduce the effect of As on the cell of the plant. On the other hand, by exposing As-stressed young trees to bacteria, the root tips developed good cell structure in comparison to those that were under As stress only. Exogenously, inoculation of bacteria clearly recuperated the damage cells observed in roots of *M. malabathricum*. These positive effects were more pronounced in A1 70 ppm As + bacteria treatment group. This finding agrees with Zeng et al. (2020) who reported no effect of inoculation of pggp on the plant root cell under cadmium (Cd). Thus, we can conclude that the application of bacteria to the plant with As stress can accelerate the ventures of the antioxidant and plays role in maintaining cellular integrity, thereby reducing the ultra-structure damage in *M. malabathricum* root tips.

### The changes in differential protein abundance in plant tissues inoculated with *M. foliorum* sp. strain SZ1

To study the variations in protein expression pattern of the plants under As stress, the two-dimensional gel electrophoresis (2DE) was conducted. Proteins partitions were conducted according to their pI value extending between pH 3 and 11. It was observed that there exists substantial amount of distinctively mass proteins amidst dissimilar experimental treatments (Fig. 6). The mean estimation of the high-quality spots was utilized as the spot capacity on the principal gel (Table 3). A 1.5-fold change in protein expression, either

**Fig. 6** 2-DE gel control and stress response images at various concentrations after 3 months



A total of 1566 protein spots  
A total of 325 differential spots  
167 down regulated and 128 upregulated spots.

---

**Table 3** A list of MS/MS-identified differentially expressed *M. malabathricum* root proteins

Spot	Accession	Description	Function	Expression Pattern	Coverage [%]	Fold	# Peptides	# PSMs	# Unique Peptides	# AAs	MW [kDa]	calc. pI	Score Sequences HT: Sequences HT
<b>As stressed treatment group vs Control</b>													
<b>Mm172</b> 2	18416218 54	Malate dehydrogenase, mitochondrial-like isoform X1 [Prunus dulcis]	Energy		18	3.4	7	160	2	340	35.4	8.47	436.93
<b>Mm179</b> 1	44906178 2	RecName: Full=Isoflavone reductase-like protein; AltName: Full=Pollen allergen Ole e 12; AltName: Allergen=Ole e 12	Energy		11	4.0	5	66	5	308	34	5.77	155.46
<b>Mm258</b> 5	18359289 92	photosystem I assembly protein Ycf4 (chloroplast) [Tinosporea sinensis]	Energy		5	4.5	1	20	1	184	21.5	9.72	45.65
<b>A1 vs A2 (70ppm)</b>													
<b>Mm239</b> 5	67038552 3	RAP domain-containing protein, chloroplastic [Zea mays]	Bioenergy and metabolism		2	1.6	1	15	1	641	71.4	5.78	30.51
<b>Mm326</b> 7	14423842	RecName: Full=Major allergen Pruar 1; AltName: Allergen=Pruar 1			8	1.5	1	84	1	160	17.3	5	202.6
<b>Mm329</b> 3	91461535 2	Nucleoside diphosphate kinase [Solanum lycopersicum]	Nucleoside metabolism		36	1.5	6	312	3	148	16.2	6.8	836.7
<b>A1 vs A2 (50ppm)</b>													
<b>Mm427</b> 6	135399	RecName: Full=Tubulin alpha-1 chain	Bioenergy and metabolism		18	1.5	7	34	2	450	49.6	5.06	74.51
<b>Mm463</b> 9	18416352 04	actin-7 [Prunus dulcis]	Cell signalling		24	1.9	7	63	1	377	41.7	5.49	164.44
<b>Mm499</b> 2	67038552 3	RAP domain-containing protein, chloroplastic [Zea mays]	Bioenergy and metabolism		2	1.9	1	11	1	641	71.4	5.78	22.51

upregulated or downregulated in at least one treatment, was considered for differential spot identification among various treatments. It was observed that about 524 spots have been found on silver-stained gels and thereof A2 with 264 spots (127 spots up-regulated and 137 spots down-regulated) by way of comparison to control following exposure to As. On the silver-stained gels, a total of 417 spots were observed and thereof, when A1 50 ppm was compared with A2 50 ppm (11 spots up-regulated and 11 spots down-regulated). Subsequently, on the silver-stained gels, spots totalling 625 were detected. In addition, A1 70 ppm was compared with A2 70 ppm (20 spots up-regulated and 19 spots down-regulated) and orbitrap (Thermo) analysis was conducted on 9 differentially expressed protein spots. It was observed that each was found to be considerably recognized as well as depicted by dart on the upper stage matchset copy produced through Progenesis Samespot software (Nonlinear Dynamic, Durham, NC) (Table 3). Six out of nine discriminatively stated recognized protein have been identified to be monitored in both treatments (As + bacteria treatment) in which, three proteins found shown in two treatments (As alone treatment) except control.

To analyze the root proteome of *M. malabathricum*, proteins were removed from *M. malabathricum* root tissue and the same amount (250 µg) of proteins had been segregated by 2-DE as mentioned in the section on Methods and Materials. Based on their functions, proteins were categorized into five main categories (Fig. 7) (Sun et al. 2016). The

proteins identified were involved in cell signaling (11%), energy metabolism (34%), defense mechanism and ROS homeostasis (22%), protein biogenesis and storage (22%), and nucleoside protein (11%) (Fig. 7).

The Venn diagram in Fig. 7 depicts the dissemination in *M. malabathricum* of distinctively expressed proteins intersecting under various exposures (control, As and As + bacteria). The regions as illustrated in the chart are disproportionate to the group’s amount of proteins. Distribution in four functional classes of 9 differentially expressed root proteins discovered by *M. malabathricum* are constructed on their assumed function denoted by the protein database use.

**Cell signaling proteins’ different appearance form**

One of the proteins was linked to cell signaling proteins’ different appearance form viz., actin (mm-4639) was identified with differential expression (1.9-fold). Actin-7 (mm-4639) also showed much profusion under As tension; however, same proteins showed low abundance when they were exposed to As and bacteria.

**Various appearance form of protein biogenesis as well as storage**

Three proteins, including two RAP domain-containing proteins, chloroplastic [Zea mays] (Mm-2395) and (Mm-4992), were identified as differential spots during As stress. Tubulin

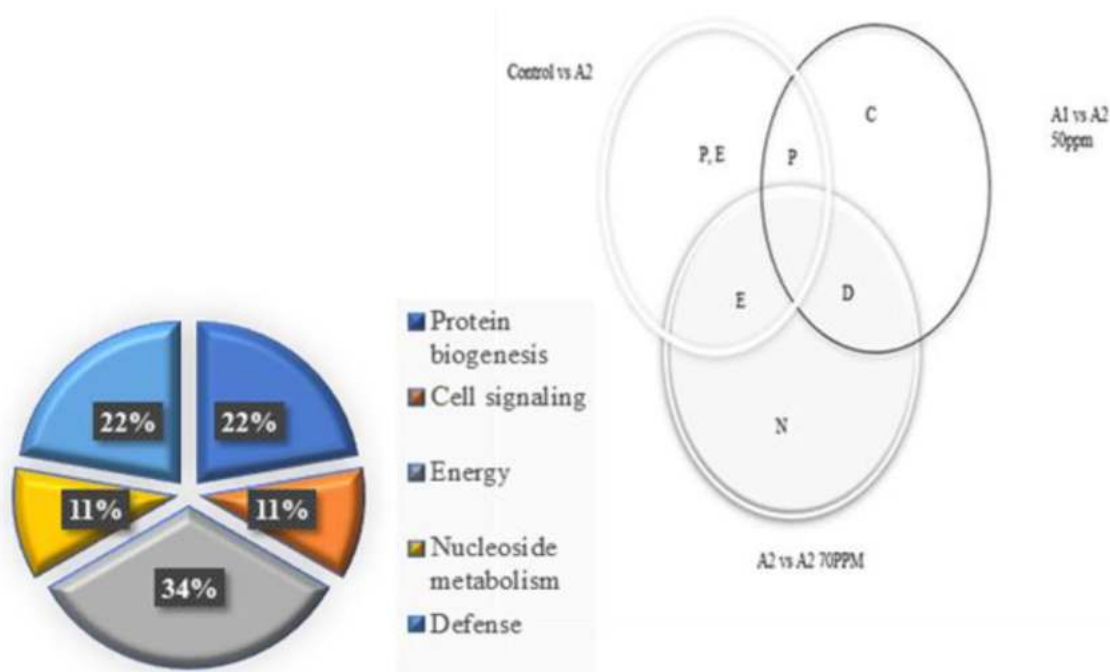


**Fig. 7** The dissemination in *M. malabathricum* of distinctively expressed proteins intersecting under various exposures (control, As and As + bacteria)

alpha-1 chain (mm-4276), were in low abundance under As stress but shows higher abundance when they were exposed to As and bacteria.

### Pattern of expression of the proteins associated with defence mechanism and ROS homeostasis

Major allergen Pru ar 1 (mm-3267) was low during As stress showing higher abundance under As + bacteria exposure.

### Proteins linked to energy metabolism had complex regulation pattern

Arsenic-exposed *M. malabathricum* root exhibited down-regulation of malate dehydrogenase (mm-1722) and photosystem I assembly protein (mm-2585) in A2 50 and were found up-regulated in A2 70, while Isoflavone reductase-like protein (mm-1791) was found up-regulated by 3.4-, 4.5- and 4.0-fold, respectively, when exposed to As alone compared with control.

### Varied expression pattern of nucleotide metabolism

Total of one protein belonged to Nucleotide metabolism, Nucleoside diphosphate kinase [*Solanum lycopersicum*] (mm-3293) was identified with differential expression (1.5-fold). Nucleoside diphosphate kinase [*Solanum lycopersicum*] (mm-3293) also displayed higher abundance when it was exposed to As and bacteria and shows low abundance compared to its exposure to As alone.

The purpose of this study was to understand the effect of *M. foliorum* sp. strain SZ1 inoculation in reducing the As toxicity in *M. malabathricum* at proteome level as well as morphology of the plant root. Plants absorb and store AsIII in their cell, a more toxic form of inorganic As that has affinity to bind with protein at the sulfhydryl group leading to inactivating of protein, enzymes and lipid peroxidation with consequent cellular damage (Alka et al. 2020, 2021; Irshad et al. 2021). AsV interferes with metabolic pathway and as a result, it has been reduced to AsIII in the cytoplasm. Several studies demonstrated that As exposure exerts negative effects on the *M. malabathricum* plants by restricting germination as well as reducing root and shoot growth, and plant biomass (Irshad et al. 2021; Patek-Mohd et al. 2018). *M. foliorum* sp. strain SZ1, a tough antagonist of As toxicity, enhances the progression of the plant under As stress. This was attributed to siderophore production, plant growth promotion in As tempted oxidative stress (Bahari et al. 2017). Physiological studies were also examined to gain a better understanding of the As + bacteria interaction. Determination of the morphological properties of plants may infer some biochemical qualities hence researchers could

determine how arsenic altered the plant's physiology. We also determine the absorption of arsenic to gain insights into basic processes, such as the bioaccumulation of arsenic in various plant parts, which have a detrimental effect on the cell structure and protein content. The results show that the plant inoculated with bacteria had a twofold increase in shoot–root length, biomass, and As uptake when compared to the other treatment group (in a separate study with no data included). That confirms the contending effects of *M. foliorum* sp. strain SZ1 on As toxicity in *M. malabathricum*.

The modifications in protein profile can cause successful adaptations that can initiate stress resistance through regulation of protein appearance and signal transition in the strain reaction. This can also directly protect the plant from stress caused by the environment (functional proteins). One cell signaling associated protein was determined as differential spots in which actin was significantly up-regulated under As stress. During As + bacteria exposure, the differential regulation of actin proteins at proteome level suggested that bacterial inoculation enhanced cell growth by controlling protein expression involved in signal transduction. Actin is an important component of plant cytoskeleton and microfilaments; it contributes to cell elongation, probably through interactions with cortical microtubules (Gupta et al. 2020a, b) and by maintaining polar auxin transport (Moussi 2020). Actin serves as the subset of microtubules and cellular microfilaments, and it assists the synthesis of cell wall and provides cell with mechanical strength (Sengupta et al. 2011). A type of the main organs for stress indication perception is roots whereby an indication machinery starts a stream expression of gene reactions to arsenic stress (Gupta et al. 2020a, b).

During As and As + bacteria exposure, the differential regulation of Tubulin proteins presumably improved cell development in *M. malabathricum*. Tubulin proteins play a crucial part in the division of cell and prolongation, while alpha-tubulin (OsC-3516) has been precisely discovered in drought tolerance rice varieties' roots (Rabello et al. 2008). Study also found that salt stress decreased tubulin abundance (Wang et al. 2008). Tubulin proteins advanced appearance trend of both level—transcriptome and proteome during As + Se exposure—showed the development and the evolution of cell will be improved by adding Se via regulation of the expression of proteins immersed in the transduction of signal (Chauhan et al. 2020).

Major allergen Pru ar 1 are defense-related proteins in plants which is a part of the Bet v 1 allergen family. It plays a significant part in the responses of the plant both to abiotic and biotic stress, as they are prompted by the two stress types (Ahammer et al 2017; Zhang et al. 2020). Major allergen takes part in abscisic acid (ABA)-activated signaling mechanism and it has great succession equivalence to pathological process linked protein (Huang et al. 2020).

The unaltered abundance or increased main allergen Pru ar 1 (G27) in 200–400  $\mu\text{M}$  *C. grandis* leaves concurred with PvPR1 in Cu-stressed *Betula pendula* and the raised abundance of Bet v 1-Sc3 (PR-10c) and bean leaves, correspondingly (Huang et al. 2020). Its up-regulation demonstrated that proteins are induced significantly by *M. foliorum* and improved the resistance of As in *M. malabathricum* correspondingly. This is similar to the findings of Zhang et al. (2020) who reported *W. anomalous* improved the resistance to disease in pear fruit which were kept under specified condition for storing the fruit. Major allergen Pru ar 1 induced in peaches by *P. membranaefaciens* (Zhang et al. 2020) in fruits by yeast (Yan et al. 2018) to enhance the defense response against pathogen.

The TCA cycle enzymes such as malate dehydrogenase (mm-1722) in plant cells partake in diverse metabolic passageways and this is governed by the location of the subcellular (Alcantara-Martinez et al. 2016). Malate dehydrogenase catalyzes the oxidations of malate resulting in oxaloacetate in citric acid pathway. These findings indicated that an increase in the accumulation of these proteins could give high-energy demand required in improving the tolerance/detoxification under abiotic stress in plants. Malate dehydrogenase, mitochondrial-like isoform X1 [*Prunus dulcis*] which catalyzes the oxidation of ester of malic acid to oxaloacetate in the final stage of the TCA cycle was down-regulated in A2 50 ppm as well as firmly adversely controlled by A2 70 ppm and this shows that the two variants modify the role of the mitochondrial. These discoveries showed that the increase in accumulation of these proteins can provide the required high-energy demand prerequisite in enhancing the tolerance/detoxification under abiotic stress in plants.

The malate dehydrogenase down-regulation could contribute to the changes seen in *M. malabathricum* photosynthetic activity as can be seen in citrus and transgenic tomato by way of mMDH reduced expression (Huang et al. 2020; Nunes-Nesi et al. 2005). Studies on the response of malate dehydrogenase in As stress (Alcántara-Martínez et al. 2018; Chauhan et al. 2020), phosphorus deficiency (Tantray et al. 2020) and under salt stress (Long et al. 2019) were reported. Malate dehydrogenase was up-regulated on day three of drought stress and continued elevated until day seven by contrast with control (Gupta et al. 2020a, b). In addition, previous research on rice stated improved malate dehydrogenase expression in drought stress (Agrawal et al. 2016). Enzyme accumulation was found to decrease in a drought-sensitive chickpea cultivar under stress at both transcript and protein levels (Subba et al. 2013). Moreover, its abundance in P-362 cultivar could be associated with its tolerance (Gupta et al. 2020a, b). Plants experiencing As stress have been shown to require a lot more energy to maintain cellular homeostasis (Chauhan et al. 2020). Since mitochondrial

ATP and TCA synthesis appear to be weakened by oxidative phosphorylation, glycolysis as well as photosynthesis produce most cellular energy, while reducing equivalents are produced in the light phase of photosynthesis and transferred through the plastidic malate–oxaloacetate shuttle to the cytosol. Under stress conditions, these mechanisms improve the antioxidant system and provide the energy requirement that could help cope with arsenic stress (Chauhan et al. 2020; Dixit et al. 2015).

Plant needs much energy under As stress to sustain cellular homeostasis as a result of over production of ROS, in which the effect on crop yield and plant biomass is seen as a crucial factor (Chauhan et al. 2020). During arsenic exposure (A2 70 ppm) (Table 3), up-regulation of all photosynthesis-related proteins might have improved carbon fixation and allowed light reaction to work effectively in order to produce more reduced equivalents. Kosova et al. (2011) associated the down-regulation of proteins involved in photosynthetic electron transport to their vulnerability to As, Cd and, (nano)silver. As a result, the transportation of electron will decline and, thus, consequently the production of ATP and NADPH will also reduce. Several lines of evidence suggest that metal-induced intracellular ROS production function in the signal transduction pathways, leading to induction of autophagy.

Isoflavone reductase also depicted variable expression pattern under As stressed compared to control. This inferred that isoflavone reductase up-regulation in As toxicity is due to not only reduced As accumulation but also increased protection in plants. Secondary metabolites play a significant role in response to external stress factors. Under metal stress, plants produce endogenous signaling molecules in which signal by ABA perception activates endogenous signal molecules, which result in regulation of the expression and activity of biosynthetic enzymes participated in secondary metabolism, leading to accumulation of target metabolites. Contingent on the states of biotic and abiotic stresses in roots, the gene in control of the synthesis of isoflavone is generated (Oliveira et al. 2020).

The accumulation of isoflavones might play an essential role in regulating the growth response. There was up-regulation of this protein due to As stress compared with the control. These proteins have been reported to increase under exposure to abiotic and biotic stress conditions (Aguilar-Galvez et al. 2020). This coincides with the finding of Farooq et al. (2018a, b), which suggested that exogenous MeJA up-regulated secondary metabolite synthesis and preserved the growth and development of *B. napus* under As exposure. *Isoflavone reductase* was found to be up-regulated in the leaves or roots of stylo under Mn toxicity (Liu et al. 2019). The proficiency rate of *isoflavone reductase* in the roots inoculated with LHL06, reported by Bilal et al. (2019) may be correlated with greater activity of *Chalcone isomerase*

in the development of flavonoids. For the biosynthesis of daidzein and conversion of stereo-specific NADPH-dependent reduction to (3R)-isoflavanone, *isoflavone reductase* is considered crucial (Bilal et al. 2019).

The only protein in the nucleotide metabolism group was *Nucleoside Diphosphate Kinase 1* (NDPK1) and was down-regulated after exposure to As. NDPK1 is a protein involved in stress response. It has a special role supplying UTP essential for cell wall precursor synthesis throughout the development of root at the initial stage and NDPK1 can be located in peroxisome, nucleus and cytosol (Štefanić et al. 2019). NDPK1 exhibits significant operational amplitude by interacting with proteins involved in a variety of processes: hormonal response, carbohydrate metabolism, signal transduction and ROS detoxification (Luzarowski et al. 2017). Nucleoside diphosphate kinase 1 overexpression can result in reduced levels of constitutive ROS and increase susceptibility to various abiotic conditions (Bona et al. 2016). Nucleoside diphosphate kinase expression has been reported to increase in response to salinity and drought, so accumulation is expected in the late stages of forming and developing of the embryo (Salekdeh and Komatsu 2007). It was found to be down-regulated with As-alone exposure compared to As + bacteria and this is in agreement with Štefanić et al. (2019) who reported after down-regulation of NDPK1 after exposure to AgNPs. Bona et al. (2016) report that by up-regulating enzymes involved in nucleotide metabolism, AM fungi change the maize proteome.

Compared with other treatment groups, the stressed arsenic group decreased protein abundance in uninoculated plants. The largest decrease in protein abundance, however, was observed under 50 ppm As stress. This may be due to decreased protein synthesis, increased protein degradation levels or both caused by abiotic stress (Bruno et al. 2020). *M. foliorum* inoculated plants exposed to As displayed greater protein abundance relative to the respective uninoculated plants (Table 3). These findings are compatible with earlier research indicating that PGPB inoculation increases the content of protein in plants under Cr (Gupta et al. 2018; Bruno et al. 2020). Protein content improvement could increase the occurrence of PGPB, which improves plants growth and biomass production under abiotic stress through various PGP processes, including P solubilization, siderophores and IAA production, which contribute to root development and metabolic activities, particularly in protein synthesis (Pandey et al. 2018). Initiation of stress-responsive machineries during environmental stimuli lead to important modification in plant proteome (Alcántara-Martínez et al. 2018). Similarly, plant microbial colonization occurs in stages that are genetically controlled (and affect the proteome of the plant) that ultimately form a firm differential form of symbiosis (Song et al. 2015). By studying such changes, it can aid in the comprehending of the adaptation mechanisms to varieties

of stress, and hence would contribute towards the enhancement of key features in plants that would be valuable for phytoremediation.

In conclusion, the proteomics-based analysis of the different expression profiles of the *M. malabathricum* root proteins provides an insight into the plant's regulatory mechanisms under As stress force and shows that at different levels of As stress, *M. malabathricum* expresses various types of proteins. Our findings also show that both components—the primary and secondary metabolic pathways of the plant—are monitored and robustly regulated under distinct magnitudes of As stress severity and are highly complex and interrelated. Specifically, proteins of root involved in ROS detoxification, root modifications, biosynthetic secondary metabolite pathways, energy metabolism and cell signaling were distinctively monitored during continuous As stress. Our statistics provide a picture of the reactions of the root of *M. malabathricum* at different levels of As or without bacterial inoculation, which could be useful for more research to have a thorough understanding of highly complex As stress reactions, including a variety of signaling pathways.

## Conclusions

The present work reports the histological and differential proteomic responses of *M. malabathricum* to determine the mechanisms of improvement mediated by PGPB As stress. PGPB as well as other microbes are associated in removing contaminants via common plants–PGPB interrelations, and hence enhancing the productivity of the plant. In addition, the histological features of root were mutually related with modifications in enhanced expression of protein immersed in As tolerance during As + bacteria exposure, defense and plant development. The energy and defense proteins which are contemplated as toolset for the adaptation in enhancement and evolution also indicated important up-regulation during As + bacteria exposure. The alterations in the expression of proteins have been authenticated via enriched expression of the related protein engaged in transport, photosynthesis, and energy pathway. The histological features as well as proteins profiling of consolidated analysis contributed towards greater comprehensions into the metabolic linkages of As + bacterial interface indicating well-tuned reaction of numerous metabolic processes to alleviate *M. malabathricum* plants of As stress.

**Acknowledgements** This research was financially supported by the Ministry of Higher Education Malaysia (Fundamental Research Grant Scheme, FRGS No. R.J130000.7854.5F102), Universiti Teknologi Malaysia (Geran Universiti Penyelidikan GUP TIER 1 No. Q.J130000.2545.17H14), and University Industry Research Laboratory, Universiti Teknologi Malaysia.

## Declarations

**Conflict of interest** The authors declare that they have no known competing financial interests or personal relationships that could have appeared to influence the work reported in this paper.

## References

- Agrawal GK, Jwa NS, Jung YH, Kim ST, Kim DW, Cho K, Shibato J, Rakwal R (2013) Rice proteomic analysis: sample preparation for protein identification. In Rice Protocols. Humana Press, Totowa, NJ, pp 151–184
- Agrawal L, Gupta S, Mishra SK, Pandey G, Kumar S, Chauhan PS, Chakrabarty D, Nautiyal CS (2016) Elucidation of complex nature of PEG induced drought-stress response in rice root using comparative proteomics approach. *Front Plant Sci* 7:1466
- Aguilar-Galvez A, Pedreschi R, Carpentier S, Chirinos R, García-Ríos D, Campos D (2020) Proteomic analysis of mashua (*Tropaeolum tuberosum*) tubers subjected to postharvest treatments. *Food Chem* 305:125485
- Ahammer L, Grutsch S, Wallner M, Ferreira F, Tollinger M (2017) NMR resonance assignments of a hypoallergenic isoform of the major birch pollen allergen Bet v 1. *Biomol NMR Assign* 11(2):231–234
- Ahmad P, Alam P, Balawi TH, Altalayan FH, Ahanger MA, Ashraf M (2020) Sodium nitroprusside (SNP) improves tolerance to arsenic (As) toxicity in *Vicia faba* through the modifications of biochemical attributes, antioxidants, ascorbate–glutathione cycle and glyoxalase cycle. *Chemosphere* 244:125480
- Ahmadpour P, Ahmadpour F, Mahmud TMM, Abdu A, Soleimani M, Tayefeh FH (2012) Phytoremediation of heavy metals: a green technology. *Afr J Biotechnol* 11(76):14036–14043
- Alcantara-Martínez N, Guizar S, Rivera-Cabrera F, Anicacio-Acevedo BE, Buendia-Gonzalez L, Volke-Sepulveda T (2016) Tolerance, arsenic uptake, and oxidative stress in *Acacia farnesiana* under arsenate-stress. *Int J Phytoremediat* 18(7):671–678
- Alcántara-Martínez N, Figueroa-Martínez F, Rivera-Cabrera F, Gutiérrez-Sánchez G, Volke-Sepúlveda T (2018) An endophytic strain of *Methylobacterium* sp. increases arsenate tolerance in *Acacia farnesiana* (L.) Willd: a proteomic approach. *Sci Total Environ* 625:762–774
- Ali B, Huang CR, Qi ZY, Ali S, Daud MK, Geng XX, Liu HB, Zhou WJ (2013) 5-Aminolevulinic acid ameliorates cadmium-induced morphological, biochemical, and ultrastructural changes in seedlings of oilseed rape. *Environ Sci Pollut Res* 20(10):7256–7267
- Alka S, Shahir S, Ibrahim N, Chai TT, Bahari ZM, Abd Manan F (2020) The role of plant growth promoting bacteria on arsenic removal: a review of existing perspectives. *Environ Technol Innov* 17:100602
- Alka S, Shahir S, Ibrahim N, Ndejiko MJ, Vo DVN, Abd Manan F (2021) Arsenic removal technologies and future trends: a mini review. *J Clean Prod* 278:123805
- Bahari ZM, Ibrahim Z, Jaafar J, Shahir S (2017) Draft genome sequence of Arsenic-resistant *Microbacterium* sp. strain SZ1 isolated from Arsenic-bearing gold ores. *Genome Announc* 5(43):2
- Barberini L, Noto A, Saba L, Palmas F, Fanos V, Dessì A, Zavattoni M, Fattuoni C, Mussap M (2016) Multivariate data validation for investigating primary HCMV infection in pregnancy. *Data Brief* 9:220–230
- Behrendt U, Ulrich A, Schumann P (2001) Description of *Microbacterium foliorum* sp. nov. and *Microbacterium phyllosphaerae* sp. nov., isolated from the phyllosphere of grasses and the surface litter after mulching the sward, and reclassification of *Aureobacterium resistens* (Funke et al. 1998) as *Microbacterium resistens* comb. nov. *Int J Syst Evol Microbiol* 51(4):1267–1276
- Bijlsma S, Bobeldijk I, Verheij ER, Ramaker R, Kochhar S, Macdonald IA, Van Ommen B, Smilde AK (2006) Large-scale human metabolomics studies: a strategy for data (pre-) processing and validation. *Anal Chem* 78(2):567–574
- Bilal S, Shahzad R, Khan AL, Al-Harrasi A, Kim CK, Lee IJ (2019) Phytohormones enabled endophytic *Penicillium funiculosum* LHL06 protects *Glycine max* L. from synergistic toxicity of heavy metals by hormonal and stress-responsive proteins modulation. *J Hazard Mater* 379:120824
- Bona E, Scarafoni A, Marsano F, Boatti L, Copetta A, Massa N, Gama-lerio E, D'Agostino G, Cesaro P, Cavaletto M, Berta G (2016) Arbuscular mycorrhizal symbiosis affects the grain proteome of *Zea mays*: a field study. *Sci Rep* 6:26439
- Bruno LB, Karthik C, Ma Y, Kadirvelu K, Freitas H, Rajkumar M (2020) Amelioration of chromium and heat stresses in Sorghum bicolor by Cr<sup>6+</sup> reducing-thermotolerant plant growth promoting bacteria. *Chemosphere* 244:
- Chandrasekhar C, Ray JG (2019) Lead accumulation, growth responses and biochemical changes of three plant species exposed to soil amended with different concentrations of lead nitrate. *Ecotoxicol Environ Saf* 171:26–36
- Chauhan R, Awasthi S, Indoliya Y, Chauhan AS, Mishra S, Agrawal L, Srivastava S, Dwivedi S, Singh PC, Mallick S, Chauhan PS (2020) Transcriptome and proteome analyses reveal selenium mediated amelioration of arsenic toxicity in rice (*Oryza sativa* L.). *J Hazard Mater* 390:122122
- Corretto E, Antonielli L, Sessitsch A, Kidd P, Weyens N, Brader G (2015) Draft genome sequences of 10 *Microbacterium* spp., with emphasis on heavy metal-contaminated environments. *Genome Announc* 3(3):e00432-e1415
- Dadransia A, Pariatamby A (2016) Phyto-enhanced remediation of soil co-contaminated with lead and diesel fuel using biowaste and *Dracaena reflexa*: a laboratory study. *Waste Manag Res* 34(3):246–253
- Das S, Jean JS, Kar S, Chou ML, Chen CY (2014) Screening of plant growth-promoting traits in arsenic-resistant bacteria isolated from agricultural soil and their potential implication for arsenic bioremediation. *J Hazard Mater* 272:112–120
- Del Giudice I, Limauro D, Pedone E, Bartolucci S, Fiorentino G (2013) A novel arsenate reductase from the bacterium *Thermus thermophilus* HB27: its role in arsenic detoxification. *Biochim Biophys Acta (BBA) Proteins Proteom* 834(10):2071–2079
- Dixit G, Singh AP, Kumar A, Dwivedi S, Deeba F, Kumar S, Suman S, Adhikari B, Shukla Y, Trivedi PK, Trivedi PK (2015) Sulfur alleviates arsenic toxicity by reducing its accumulation and modulating proteome, amino acids and thiol metabolism in rice leaves. *Sci Rep* 5:16205
- Farnese FS, Oliveira JA, Paiva EA, Menezes-Silva PE, da Silva AA, Campos FV, Ribeiro C (2017) The involvement of nitric oxide in integration of plant physiological and ultrastructural adjustments in response to arsenic. *Front Plant Sci* 8:516
- Farooq MA, Gill RA, Ali B, Wang J, Islam F, Ali S, Zhou W (2016) Subcellular distribution, modulation of antioxidant and stress-related genes response to arsenic in *Brassica napus* L. *Ecotoxicology* 25(2):350–366
- Farooq MA, Zhang K, Islam F, Wang J, Athar HU, Nawaz A, Ullah Zafar Z, Xu J, Zhou W (2018a) Physiological and iTRAQ-based quantitative proteomics analysis of methyl jasmonate-induced tolerance in *Brassica napus* under arsenic stress. *Proteomics* 18(10):1700290
- Farooq MA, Islam F, Yang C, Nawaz A, Gill RA, Ali B, Song W, Zhou W (2018b) Methyl jasmonate alleviates arsenic-induced oxidative damage and modulates the ascorbate–glutathione cycle in oilseed rape roots. *Plant Growth Regul* 84(1):135–148

- Fru EC, Callac N, Posth NR, Argyraki A, Ling YC, Ivarsson M, Broman C, Kiliyas SP (2018) Arsenic and high affinity phosphate uptake gene distribution in shallow submarine hydrothermal sediments. *Biogeochemistry* 141(1):41–62
- Fu HL, Meng Y, Ordóñez E, Villadangos AF, Bhattacharjee H, Gil JA, Mateos LM, Rosen BP (2009) Properties of arsenite efflux permeases (Acr3) from *Alkaliphilus metalliredigens* and *Corynebacterium glutamicum*. *J Biol Chem* 284(30):19887–19895
- Ghosh A, Pramanik K, Bhattacharya S, Mondal S, Ghosh SK, Ghosh PK, Maiti TK (2021) Abatement of arsenic-induced phytotoxic effects in rice seedlings by an arsenic-resistant *Pantoea dispersa* strain. *Environ Sci Pollut Res* 28(17):21633–21649
- Gupta P, Kumar V, Usmani Z, Rani R, Chandra A, Gupta VK (2020a) Implications of plant growth promoting *Klebsiella* sp. CPSB4 and *Enterobacter* sp. CPSB49 in luxuriant growth of tomato plants under chromium stress. *Chemosphere* 240:124944
- Gupta P, Rani R, Chandra A, Kumar V (2018) Potential applications of *Pseudomonas* sp. (strain CPSB21) to ameliorate Cr<sup>6+</sup> stress and phytoremediation of tannery effluent contaminated agricultural soils. *Sci Rep* 8(1):1–10
- Gupta S, Mishra SK, Misra S, Pandey V, Agrawal L, Nautiyal CS, Chauhan PS (2020b) Revealing the complexity of protein abundance in chickpea root under drought-stress using a comparative proteomics approach. *Plant Physiol Biochem* 15:88–102
- Hackstadt AJ, Hess AM (2009) Filtering for increased power for microarray data analysis. *BMC Bioinform* 10(1):11
- Hall JA (2002) Cellular mechanisms for heavy metal detoxification and tolerance. *J Exp Bot* 53(366):1–11
- Huang WL, Wu FL, Huang HY, Huang WT, Deng CL, Yang LT, Huang ZR, Chen LS (2020) Excess copper-induced alterations of protein profiles and related physiological parameters in citrus leaves. *Plants* 9(3):291
- Irshad S, Xie Z, Mehmood S, Nawaz A, Ditta A, Mahmood Q (2021) Insights into conventional and recent technologies for arsenic bioremediation: a systematic review. *Environ Sci Pollut Res* 28(15):18870–18892
- Khan DH, Duckett JG, Frankland B, Kirkham JB (1984) An X-ray microanalytical study of the distribution of cadmium in roots of *Zea mays* L. *J Plant Physiol* 115(1):19–28
- Khan KY, Ali B, Stoffella PJ, Cui X, Yang X, Guo Y (2020) Study amino acid contents, plant growth variables and cell ultrastructural changes induced by cadmium stress between two contrasting cadmium accumulating cultivars of *Brassica rapa* ssp. *chinensis* L. (pak choi). *Ecotoxicol Environ Saf* 200:110748
- Kleinknecht L, Wang F, Stübe R, Philippar K, Nickelsen J, Bohne AV (2014) RAP, the sole octotricopeptide repeat protein in *Arabidopsis*, is required for chloroplast 16S rRNA maturation. *Plant Cell* 26(2):777–787
- Kosová K, Vítámvás P, Prášil IT, Renaut J (2011) Plant proteome changes under abiotic stress—contribution of proteomics studies to understanding plant stress response. *J Proteom* 74(8):1301–1322
- Lindsay ER, Maathuis FJ (2017) New molecular mechanisms to reduce arsenic in crops. *Trends Plant Sci* 22(12):1016–1026
- Liu P, Huang R, Hu X, Jia Y, Li J, Luo J, Liu Q, Luo L, Liu G, Chen Z (2019) Physiological responses and proteomic changes reveal insights into *Stylosanthes* response to manganese toxicity. *BMC Plant Biol* 19(1):212
- Long R, Li M, Zhang T, Kang J, Sun Y, Yang Q (2019) Comparative proteomic analysis reveals differential root proteins in *Medicago sativa* and *Medicago truncatula* in response to salt stress. In: de Bruijn FJ (ed) *The model legume Medicago truncatula*. Wiley, New York, pp 1102–1111
- Luzarowski M, Kosmacz M, Sokolowska E, Jasińska W, Willmitzer L, Veyel D, Skirycz A (2017) Affinity purification with metabolomic and proteomic analysis unravels diverse roles of nucleoside diphosphate kinases. *J Exp Bot* 68(13):3487–3499
- Moussi CJ (2020) Transforming growth factor-beta targets Formin-like 2 for Angiopoietin-like 4 secretion during the epithelial mesenchymal transition. Doctoral dissertation, Philipps-Universität Marburg
- Mukherjee G, Saha C, Naskar N, Mukherjee A, Mukherjee A, Lahiri S, Majumder AL, Seal A (2018) An endophytic bacterial consortium modulates multiple strategies to improve arsenic phytoremediation efficacy in *Solanum nigrum*. *Sci Rep* 8(1):6979
- Nunes-Nesi A, Carrari F, Lytovchenko A, Smith AM, Loureiro ME, Ratcliffe RG, Sweetlove LJ, Fernie AR (2005) Enhanced photosynthetic performance and growth as a consequence of decreasing mitochondrial malate dehydrogenase activity in transgenic tomato plants. *Plant Physiol* 137(2):611–622
- Oliveira BRM, de Almeida AAF, Pirovani CP, Barroso JP, Neto CHDC, Santos NA, Ahnert D, Baligar VC, Mangabeira PAO (2020) Mitigation of Cd toxicity by Mn in young plants of cacao, evaluated by the proteomic profiles of leaves and roots. *Ecotoxicology* 29(3):340–358
- Pandey AS, Sharma E, Jain N, Singh B, Burman N, Khurana JP (2018) A rice bZIP transcription factor, OsbZIP16, regulates abiotic stress tolerance when over-expressed in Arabidopsis. *J Plant Biotechnol* 27(4):393–400
- Pandey N, Manjunath K, Sahu K (2020) Screening of plant growth promoting attributes and arsenic remediation efficacy of bacteria isolated from agricultural soils of Chhattisgarh. *Arch Microbiol* 202(3):567–578
- Patek-Mohd NN, Abdu A, Jusop S, Abdul-Hamid H, Karim M, Nazrin M, Akbar MH, Jamaluddin AS (2018) Potentiality of *Melastoma malabathricum* as phytoremediators of soil contaminated with sewage sludge. *Sci Agricola* 75(1):27–35
- Perez-Riverol Y, Csordas A, Bai J, Bernal-Llinares M, Hewapathirana S, Kundu DJ, Inuganti A, Griss J, Mayer G, Eisenacher M, Pérez E (2019) The PRIDE database and related tools and resources in 2019: improving support for quantification data. *Nucleic Acids Res* 47(D1):D442–D450
- Rabello AR, Guimarães CM, Rangel PH, da Silva FR, Seixas D, de Souza E, Brasileiro AC, Spehar CR, Ferreira ME, Mehta A (2008) Identification of drought-responsive genes in roots of upland rice (*Oryza sativa* L). *BMC Genom* 9(1):485
- Rajoo K, Abdu A, Singh D, Abdul-Hamid H, Jusop S, Zhen W (2013) Heavy metal uptake and translocation by *Dipterocarpus verrucosus* from sewage sludge contaminated soil. *Am J Environ Sci* 9(3):259–268
- Salekdeh GH, Komatsu S (2007) Crop proteomics: aim at sustainable agriculture of tomorrow. *Proteomics* 7(16):2976–2996
- Samrana S, Ali A, Muhammad U, Azizullah A, Ali H, Khan M, Naz S, Khan MD, Zhu S, Chen J (2020) Physiological, ultrastructural, biochemical, and molecular responses of glandless cotton to hexavalent chromium (Cr<sup>6+</sup>) exposure. *Environ Pollut* 266:115394
- Sengupta D, Kannan M, Reddy AR (2011) A root proteomics-based insight reveals dynamic regulation of root proteins under progressive drought stress and recovery in *Vigna radiata* (L.) Wilczek. *Planta* 233(6):1111–1127
- Song F, Qi D, Liu X, Kong X, Gao Y, Zhou Z, Wu Q (2015) Proteomic analysis of symbiotic proteins of *Glomus mosseae* and *Amorpha fruticosa*. *Sci Rep* 5:18031
- Squibb KS, Fowler BA (1983) The toxicity of arsenic and its compounds. In: Fowler BA (ed) *Biological and environmental effects of arsenic*, pp 233–269
- Srivastava S, Suprasanna P, D'Souza SF (2011) Redox state and energetic equilibrium determine the magnitude of stress in *Hydrilla verticillata* upon exposure to arsenate. *Protoplasma* 248(4):805–815

- Štefanić PP, Jarnević M, Cvjetko P, Biba R, Šikić S, Tkalec M, Cindrić M, Letofsky-Papst I, Balen B (2019) Comparative proteomic study of phytotoxic effects of silver nanoparticles and silver ions on tobacco plants. *Environ Sci Pollut Res* 26(22):22529–22550
- Subba P, Kumar R, Gayali S, Shekhar S, Parveen S, Pandey A, Datta A, Chakraborty S, Chakraborty N (2013) Characterisation of the nuclear proteome of a dehydration-sensitive cultivar of chickpea and comparative proteomic analysis with a tolerant cultivar. *Proteomics* 13(12–13):1973–1992
- Tantray AY, Ali HM, Ahmad A (2020) Analysis of proteomic profile of contrasting phosphorus responsive rice cultivars grown under phosphorus deficiency. *Agronomy* 10(7):1028
- Titah HS, Abdullah SRS, Mushrifah I, Anuar N, Basri H, Mukhlisin M (2013) Effect of applying rhizobacteria and fertilizer on the growth of *Ludwigia octovalvis* for arsenic uptake and accumulation in phytoremediation. *Ecol Eng* 58:303–313
- Tlustoš P, Goessler W, Száková J, Balík J (2002) Arsenic compounds in leaves and roots of radish grown in soil treated by arsenite, arsenate and dimethylarsinic acid. *Appl Organomet Chem* 16(4):216–220
- Van den Berg RA, Hoefsloot HC, Westerhuis JA, Smilde AK, van der Werf MJ (2006) Centering, scaling, and transformations: improving the biological information content of metabolomics data. *BMC Genom* 7(1):142
- Veza ME, Nicotra MFO, Agostini E, Talano MA (2020) Biochemical and molecular characterization of arsenic response from *Azospirillum brasilense* Cd, a bacterial strain used as plant inoculant. *Environ Sci Pollut Res* 27(2):2287–2300
- Wang MC, Peng ZY, Li CL, Li F, Liu C, Xia GM (2008) Proteomic analysis on a high salt tolerance introgression strain of *Triticum aestivum*/*Thinopyrum ponticum*. *Proteomics* 8(7):1470–1489
- Wang P, Chen X, Xu X, Lu C, Zhang W, Zhao FJ (2018) Arsenate induced chlorosis 1/translocon at the outer envelope membrane of chloroplasts 132 protects chloroplasts from arsenic toxicity. *Plant Physiol* 178(4):1568–1583
- Wheelock AM, Wheelock CE (2013) Trials and tribulations of 'omics data analysis: assessing quality of SIMCA-based multivariate models using examples from pulmonary medicine. *Mol BioSyst* 9(11):2589–2596
- Worley B, Powers R (2013) Multivariate analysis in metabolomics. *Curr Metabolomics* 1(1):92–107
- Xia J, Sinelnikov IV, Han B, Wishart DS (2015) MetaboAnalyst 3.0—making metabolomics more meaningful. *Nucleic Acids Res* 43(W1):W251–W257
- Yan Y, Zhang X, Zheng X, Apaliya MT, Yang Q, Zhao L, Xu W, Feng L, Ma M, Zhu YG, Zhang H (2018) Control of postharvest blue mold decay in pears by *Meyerozyma guilliermondii* and its effects on the protein expression profile of pears. *Postharvest Biol Technol* 136:124–131
- Zaheer IE, Ali S, Saleem MH, Imran M, Alnusairi GS, Alharbi BM, Riaz M, Abbas Z, Rizwan M, Soliman MH (2020) Role of iron–lysine on morpho-physiological traits and combating chromium toxicity in rapeseed (*Brassica napus* L.) plants irrigated with different levels of tannery wastewater. *Plant Physiol Biochem* 155:70–84
- Zeng X, Pang L, Chen Y, Kong X, Chen J, Tian X (2020) Bacteria *Sphingobium yanoikuyae* Sy 310 enhances accumulation capacity and tolerance of cadmium in *Salix matsudana* Koidz roots. *Environ Sci Pollut Res* 27(16):19764–19773
- Zhang X, Wu F, Gu N, Yan X, Wang K, Dhanasekaran S, Gu X, Zhao L, Zhang H (2020) Postharvest biological control of Rhizopus rot and the mechanisms involved in induced disease resistance of peaches by *Pichia membranefaciens*. *Postharvest Biol Technol* 163:111146
- Zhou C, Huang M, Li Y, Luo J, Cai L (2016) Changes in subcellular distribution and antioxidant compounds involved in Pb accumulation and detoxification in *Neyraudia reynaudiana*. *Environ Sci Pollut Res* 23(21):21794–21804
- Zvobgo G, LwalabaWaLwalaba J, Sagonda T, Mapodzeke JM, Muhammad N, Shamsi IH, Zhang G (2018) Phosphate alleviates arsenate toxicity by altering expression of phosphate transporters in the tolerant barley genotypes. *Ecotoxicol Environ Saf* 147:832–839